The variety of subaerial active salt deformations in the Kuqa fold-thrust belt (China) constrained by InSAR

Cindy Colón, A. Alexander G. Webb, Cécile Lasserre, Marie-Pierre Doin,
Francois Renard, Rowena Lohman, Jianghai Li, Patrick F. Baudoin

1   **The variety of subaerial active salt deformations in the Kuqa fold-thrust belt**

2   **(China) constrained by InSAR**

3

4   Cindy Colón[1*], A. Alexander G. Webb[2], Cécile Lasserre[3,4], Marie-Pierre Doin[3,4],

5   François Renard[3,4,5], Rowena Lohman[6], Jianghai Li[7], Patrick F. Baudoin[1]

6

7

8   *[1]Department of Geology and Geophysics, Louisiana State University, Baton Rouge,*

9   *Louisiana, 70803, USA*

10 *[2] Department of Earth Sciences, University of Hong Kong, Hong Kong, China*

11 *[3]ISTerre, University Grenoble Alpes, BP53, 38041, Grenoble, Cedex 09, France*

12 *[4]ISTerre, CNRS, BP53, 38041, Grenoble, Cedex 09, France*

13 *[5]PGP, Dept. Geosciences, University of Oslo, box 1048, Blindern, 0316 Oslo, Norway*

14 *[6]Earth and Atmospheric Sciences, Cornell University, Ithaca, New York, 14850, USA*

15 *[7]The Key Laboratory of Orogenic Belts and Crustal Evolution, Ministry of Education,*

16 *School of Earth and Space Sciences, Peking University, Beijing 100871, China*

17

18

19

20 *Corresponding author: cincolon@gmail.com

21

22

26 **ABSTRACT**

27   **Surface salt bodies in the western Kuqa fold-thrust belt of northwestern**

28 **China allow study of subaerial salt kinematics and its possible correlations with**

29 **weather variations. Ephemeral subaerial salt exposure during the evolution of a salt**

30 **structure can greatly impact the subsequent development and deformation of its**

31 **tectonic setting. Here, we present a quantitative time-lapse survey of surface salt**

32 **deformation measured from interferometric synthetic aperture radar (InSAR) using**

33 **Envisat radar imagery acquired between 2003 and 2010. Time series analysis and**

34 **inspection of individual interferograms confirm that the majority of the salt bodies**

35 **in western Kuqa are active, with significant InSAR observable displacements at 3 of**

36 **4 structures studied in the region. Subaerial salt motion toward and away from the**

37 **satellite at rates up to 5 mm/yr with respect to local references. Rainfall**

38 **measurements from the Tropical Rainfall Measuring Mission (TRMM) and**

39 **temperature from a local weather station are used to test the relationship between**

40 **seasonality and surface salt motion. We observe decoupling between surface salt**

41 **motion and seasonality and interpret these observations to indicate that regional**

42 **and local structural regimes exert primary control on surface salt displacement**

43 **rates.**

44

45 **Key words:** Kuqa fold-thrust belt, salt deformation, namakiers, InSAR

46

47

48

1. INTRODUCTION

Analysis of subaerial salt behavior is limited because allochthonous salt outcrops are rarely preserved on the Earth's surface, making subsurface imaging the primary technique for observing salt deposits (Talbot and Pohjola, 2009). Few examples of salt bodies outcrop at the surface today (Zagros, Iran; Salt Range, Pakistan), not including submarine salt exposures. Interpretations of many subsurface salt bodies throughout the world have indicate subaerial exposure during structural evolution (e.g., Canerot et al., 2005). This subaerial exposure may be short-lived and yet have key impacts on the long-term evolution because salt bodies interacting with surface processes may display sharply distinct kinematics versus subsurface salt bodies. As a result, it is important for the overall exploration of crustal salt to study the few available subaerial salt bodies. Many structural systems dominated by salt deformation are commonly associated with major hydrocarbon reservoirs. Additional compelling reasons to explore subaerial salt bodies are (1) distinctive mechanical properties of salt make it one of the few solid Earth materials able to flow at the surface, and (2) these represent Earth-surface deformation systems that can be highly responsive to weather conditions (Talbot and Rogers, 1980).

Much of our current understanding of surface salt kinematics stems from namakier (extrusive salt "glaciers", also called "salt fountains") studies predominantly in the Alborz and Zagros Mountains in northern and southern Iran, respectively (e.g., Kent, 1979). Over one hundred Hormuz salt diapirs, fed from pipe-like conduits (point-sourced), are known to exist in the Zagros Mountains (Kent, 1979). Of these salt bodies, surface motion has been observed on twenty diapirs using a satellite-based remote sensing technique called interferometry of synthetic aperture radar (InSAR) capable of

72   measuring millimeter-scale vertical displacements (Barnhart and Lohman, 2012). The

73   sheet-like Garmsar salt nappe of the Alborz Mountains extruded along a frontal thrust

74   before undergoing open-toed advance and is presently inactive; the motion detected by

75   InSAR is attributed to dissolution (Baikpour et al., 2010). Furthermore, InSAR has also

76   been used to detect continuous vertical, upward flow rates between 5.5-8.3 mm/yr across

77   the line-sourced Sedom diapir in the Dead Sea basin (Weinberger et al., 2006).

78   Recently recognized namakiers in the western Kuqa fold-thrust belt in

79   northwestern China provide a new natural laboratory to observe and constrain subaerial

80   salt kinematics (Li et al., 2014). Four active point-sourced namakiers exist in western

81   Kuqa fold-thrust belt (**Figure 1**). An active line-sourced diapir, the Tuzimazha salt wall,

82   is comparable to the Sedom diapir with vertical, upward flow. Quele namakier, exposed

83   in western Kuqa fold-thrust belt, is an active open-toed, line-sourced subaerial salt

84   structure extruded from a surface-breaching thrust fault on Earth's surface. Kuqa fold-

85   thrust belt provides an invaluable opportunity to study the behavior of a variety of

86   subaerial salt bodies within the same geologic setting. Furthermore, the Kuqa fold-thrust

87   belt is more accessible than other examples of subaerial salt extrusion like the Salt Range

88   of Pakistan.

89   Existing work concludes that the presence of meteoric water and fluctuating

90   temperatures are the principal factors enabling salt recrystallization and/or dissolution

91   after surface extrusion (Talbot and Rogers, 1980; Urai et al., 1986; Desbois et al., 2010).

92   In the present study, we use InSAR to measure the spatial and temporal deformation

93   patterns of namakiers in Kuqa fold-thrust belt. We compare these observations to rainfall

94   and temperature measurements in order to explore potential relationships between the

95   active surface salt kinematics and local weather conditions.

96   **2. BACKGROUND**

97   **2.1 Geologic setting**

98   The Kuqa foreland fold-thrust belt actively accommodates ~4-7 mm/yr of north-

99   south tectonic shortening between the Tian Shan to the north and the Tarim basin to the

100   south across a ~400 km long, ~20-65 km wide region (e.g., Allen et al., 1991).

101   Contractional tectonics have formed structural hydrocarbon traps across Kuqa fold-thrust

102   belt where the deformational style is controlled by the presence and varying thickness of

103   salt layers (e.g. Tang et al., 2004; Chen et al., 2004). The subsalt sequence (Upper

104   Permian-Cretaceous) includes Triassic-Jurassic coal and lacustrine mudstones that

105   matured into regional hydrocarbon source rocks (Hendrix et al., 1992; Tang et al., 2004;

106   Chen et al., 2004). Two salt dominated units control deformation across Kuqa (Li et al.,

107   2012): the Miocene Jidike Formation and Paleocene-Eocene Kumugeliemu Group

108   concentrated in eastern and western Kuqa, respectively. The Kumugeliemu Group

109   consists of halite and gypsum interbedded with mudstone, sandstone, conglomerate and

110   marl (Hendrix et al., 1992; Chen et al., 2004). These strata had an original thickness of

111   ~1100 m and the range of current thicknesses spans 110-3000 m (Hendrix et al., 1992;

112   Chen et al., 2004; Yixin and Pengwan, 2009). This dramatic thickness range testifies to

113   the importance of salt flow, which thinned and thickened the unit laterally. Where the salt

114   units thicken toward the south, deformation is concentrated in the suprasalt sequence.

115   From west to east, salt décollements in Kuqa fold-thrust belt have developed into salt

116   nappes exposed at the surface, triangle zones and pop-up structures (Chen et al., 2004;

117   Wang et al., 2011, Li et al., 2012). The suprasalt sequence (Oligocene-Quaternary)

118   reaches a thickness of ~7 km (Tang et al., 2004; Li et al., 2014). The salt-dominated

119   Kumugeliemu Group in western Kuqa fold-thrust belt (**Figure 1**) outcrops at line-sourced

120   and point-sourced salt structures. These surface salt structures display structural and

121   stratigraphic records of active vertical motion, exhumation and surface flow (Li et al.,

122   2014).

123   Point-sourced salt structures, like Awate namakier, Bozidun namakier and an

124   unspecified structure referred to hereafter as Daxiagu namakier, are fed from a salt source

125   via pipe-like feeders (i.e., stems) (e.g., Jackson and Talbot, 1986). Awate namakier

126   occurs at the western extent of the Quilitage anticline system, divided by a south-flowing

127   river. The eastern portion of Awate namakier is approximately 2.5 km long and 1.5 km

128   wide. The western portion may have the same salt source (Li et al., 2014). Salt mining at

129   the southern edge of Awate exposes freshly cut outcrop surfaces and reveals a mud-rich,

130   1-3 m thick carapace above the namakier. Bozidun namakier is located ~17 km north of

131   Awate with a length of ~2.2 km and 1.4 km width. Lastly, Daxiagu namakier is the

132   westernmost surface salt structure in Kuqa, located ~12 km west-northwest of Awate.

133   Daxiagu is ~4.5 km long and 3.4 km wide and we interpret it to be a point-sourced based

134   on its circumscribed surface geometry.

135   Line-sourced salt structures such as Quele namakier and Tuzimazha salt wall have

136   relatively thin, elongated salt feeders (e.g., Jackson and Talbot, 1986). The Quele salt

137   thrust propagates southward and the salt décollement is exhumed where the thrust fault

138   intersects the surface, forming the Quele namakier. Quele namakier is exposed across

139   ~32 km E-W with a vertical thickness generally ranging from ~50-200 m. The namakier

140 thins and locally pinches out toward the west and the salt thrust extends to a north-

141 trending, salt-lubricated strike-slip fault that appears to transfer slip to another E-W

142 trending thrust fault further north (Zhong and Xia, 1998a; Li et al., 2014). Quele

143 namakier broadens at its eastern extent and covers an area ~5km wide, called the

144 Chaerhan namakier, which also features an isolated salt dome (Li et al., 2014). Large,

145 siliciclastic rock bodies, of varying sizes reaching up to 2.5 km length, occur across

146 Quele namakier. These rock bodies may be considered rafts if that have been dislodged

147 from surrounding sedimentary units and incorporated into the namakier as it flows. These

148 sedimentary bodies may also be the more brittle, siliciclastic rocks that make up the

149 Kumugeliemu Group. Toward the north in the hinterland of Kuqa, the subvertical

150 Tuzimazha salt wall trends east-southeast and maintains an ~50 m thickness along its ~10

151 km long surface exposure.

152 **2.2 Subaerial salt deformation and the impact of weather conditions**

153   Relatively low viscosity and density as well as a strong resistance to compression

154 allows rock salt to flow as a non-Newtonian fluid that can pierce through surrounding

155 sedimentary layers in the Earth's upper crust (e.g., Weijermars et al., 1993).

156 Microstructural analysis shows that salt flow converges and accelerates as it moves from

157 a buried source layer into a diapiric feeder, or stem (Desbois et al., 2010). The principal

158 deformation mechanisms observed at the stem of the diapir are grain-boundary migration

159 (GBM) and sub-grain rotation (SGR) caused by increased differential stress (Desbois et

160 al., 2010). Exhumation of salt initially forms salt domes that later develop into salt

161 fountains as circumferential lateral spreading propagates away from the orifice (e.g.,

162 Kehle, 1988). Dominant deformation mechanisms shift from GBM and SGR to pressure-

163   solution accommodated grain-boundary sliding (GBS) from the top to the distal part of

164   the salt fountain (Desbois et al., 2010). This shift can be explained by the influx of

165   meteoric water and the decreased differential stress as salt flow divergences radially away

166   from the orifice (i.e., Jackson, 1985; Desbois et al., 2010). A ground-based geodetic

167   study, with hourly to daily sampling, of the Kuh-e-Namak namakier in southern Iran

168   proposed that the presence of meteoric water causes plastic deformation of the salt while

169   daily temperature variations cause elastic deformation (Talbot and Rogers, 1980).

170   Temporary surface salt flow rate of ~500 mm/day was observed at Kuh-e-Namak

171   namakier shortly after a large rain event (~330 mm average rainfall from October to

172   February) (Talbot and Rogers, 1980). Furthermore, it was observed that during dry

173   periods the surface salt shrunk, retreating and losing some of lateral extent attained

174   during the wet period (Talbot and Rogers, 1980).

175   Given the typical low-pressure stress conditions of subaerial salt bodies, the

176   namakier porosity is stimulated by joints formed as a result of diurnal/seasonal thermal

177   expansion and contraction (Merriam et al., 1962; Talbot and Aftabi, 2004; Desbois et al.,

178   2010). Vertical joints in subaerial salt bodies dilate as the salt carapace spreads in

179   response to continual growth of the viscous salt fountain, which permits infiltration of

180   meteoric water (Desbois et al., 2010). The carapace of a namakier is typically composed

181   of granular clastic material left behind after the shallower layers of salt have dissolved

182   (e.g., Walker 1973). An annual temperature range of -0.5°C to 37.8°C was enough to

183   facilitate the plastic deformation observed at Kuh-e-Namak (Talbot and Rogers, 1980).

184   However, surface motion during dry periods not only depends on temperature but also the

185   thermal gradient in the salt, which is dependent on the wetness of the salt (Talbot and

186 Rogers, 1980). The semi-arid climate of the Kuqa fold-thrust belt allows the preservation

187 of subaerial salt exposures. Here, annual rainfall averages ~74 mm (April-October) and

188 average temperatures can range from -13.3°C to 31.2°C.

189 **2.3 Models, predictions, and tests**

190   The rapid kinematic response of surface salt structures to temporary stimuli

191 requires subaerial salt evolution analysis to consider short-term (days to years)

192 deformation kinematics. The rates of salt supply, salt dissolution, sediment accumulation

193 of the overburden, erosion and regional tectonic strain influence the long-term evolution

194 of a namakier (i.e., Koyi, 1998; McGuinness and Hossack, 1993). Crustal shortening may

195 impede diapirism if lateral compression results in an obstruction of the salt feeder (Koyi,

196 1998). In other circumstances the compression of a diapir feeder may physically separate

197 the diapir from the source layer. This can produce a temporary pulse of increased salt

198 extrusion rates that would mark the onset of the final phases of namakier evolution (Koyi,

199 1998).

200   Extreme daily temperature variations in semi-arid climates, like Kuqa fold-thrust

201 belt, lead to oscillating inflation and deflation of a subaerial salt body on a sub-hourly to

202 daily scale (Talbot and Rogers 1980). We would expect the entire surface of the

203 namakiers to uplift during daylight hours, when surface temperatures can be very high,

204 under the influence of thermal expansion (Merriam et al., 1962). Similarly, we expect

205 subsidence across the namakier surfaces, as a result of thermal contraction, when

206 temperatures drop well below freezing. Hourly sampling, at minimum, of temperature

207 and surface motion would be necessary to detect the rate and degree of daily oscillations

208 across the namakier surfaces at Kuqa fold-thrust belt. Similar inflation and deflation

209   cycles in response to seasonal variations may also be detectable. However all these

210   variations due to the thermal expansion or contraction of the salt body are likely small

211   because the coefficient of the very low thermal expansion of NaCl, in the range of 5.10^{-6}

212    $°C^{-1}$ (White, 1965). For example, in the idealized case of a homogeneous variation of

213   40°C on a 1 meter thick salt layer, these thermal effects would result in a vertical

214   displacement of the order of 200 micrometers.

215   The short-term deformation patterns of namakiers must consider moisture at the

216   surface. When sufficient quantities of meteoric water make contact with/infiltrate

217   namakiers, pressure-solution and grain boundary sliding allow accelerated salt flow. We

218   expect namakiers at Kuqa fold-thrust belt to flow faster within days after storm and rain

219   events. As salt flow accelerates the leading edge of the surface salt bodies should extend

220   further laterally. As a namakier spreads laterally, the surface should appear to subside.

221   This can be visualized for a static namakier by considering how a drop of molasses would

222   behave on a tabletop. As the drop spreads slowly in every direction, the surface will

223   flatten, bringing the top of the molasses closer to the table.

224   Two models suggest conflicting roles of the carapace in surface salt kinematics

225   during dry periods. One scenario is the dry-inflation model that suggests the carapace that

226   develops on a surface salt body inhibits lateral spreading and facilitates swelling at the

227   dome (above the orifice) as the salt extrudes from the feeder (Talbot and Pohjola, 2009).

228   If this model holds for Kuqa fold-thrust belt then we should see a relative surface uplift

229   above the orifice during dry periods. Alternatively, dry-deflation model suggests that the

230   carapace hinders uplift of the central dome and instead promotes lateral spreading (Aftabi

231   et al., 2010). With a constant salt supply rate, this model suggests a continual surface

232   subsidence of the namakier as it spreads laterally. To test these models we must record

233   time-lapse surface motions of the Kuqa fold-thrust belt namakiers during wet and dry

234   periods as well as document the occurrences of rain events.

235   The resistance supplied by a load overlying the orifice of a namakier is another

236   factor that can potentially impact subaerial salt. Emergent, surface breaching, diapirs rise

237   faster than pre-emergent diapirs because of the reduced confinement and load when the

238   overburden is removed (e.g., Weinberg, 1993). Strain rates from microstructural analysis

239   for pre-emergent diapirs range from 10^{-15} to 10^{-13} s^{-1} while higher strain rates from 10^{-11}

240   to 10^{-9} s^{-1} have been observed for emergent diapirs (Talbot and Jackson, 1987). This

241   aligns with flow velocity estimates that show pre-emergent diapirs in Germany rise ~0.3

242   mm/yr while emergent diapirs in Iran can exceed 10 mm/yr (e.g., Trusheim, 1960; Talbot

243   and Aftabi, 2004). Strain and velocity rates of pre-emergent and emergent diapirs

244   reasonably suggest that the rate of salt extrusion can increase if enough material above

245   the orifice of a namakier is removed. The salt above the orifice is a load, and this load is

246   reduced by salt spreading away from the orifice at the surface.

247   Removal of material above the orifice can occur via erosion and salt dissolution.

248   During periodic large storm events, the shallow, relatively uncompact layers of the

249   namakier carapace can erode considerably (Wenkert, 1979). Furthermore, significant salt

250   dissolution can occur during storm events if the carapace thickness allows sufficient

251   meteoric water to infiltrate the namakier. In the event that the removal of material above

252   the orifice is large enough, we expect acceleration of salt extrusion resulting in an overall

253   rise of the namakier surface. Conversely, if the load above the namakier orifice controls

254   the salt extrusion rate, a thickening carapace would cause a deceleration of salt extrusion

255   that would also lead to a deceleration of lateral spreading.

256   **3. METHODS**

257   To better understand the complex set of processes that govern deformation in salt

258   bodies, we examine several different bodies using a diverse set of data, including space-

259   based constraints on ground deformation and weather information from both ground

260   stations and remote sensing. Surface salt deformation is accessed using a remote sensing

261   technique called interferometry of synthetic aperture. To perform the InSAR analysis we

262   utilize Envisat ASAR (Advanced Synthetic Aperture Radar) imagery acquired between

263   June 2003 and October 2010. To access the relationship between subaerial salt motions

264   and weather conditions we use Tropical Rainfall Measuring Mission (TRMM) data and

265   local weather station data during the same period of Envisat acquisitions. The temporal

266   resolution of the Envisat imagery available must be less than the temporal range of

267   surface salt motion to detect the salts' kinematic responses to weather variations (**Figure

268   3**). Because of this it is unlikely that our Envisat dataset could resolve the impact of

269   individual storm events as our best temporal resolution is 36 days. However, it is possible

270   to detect the impact of seasonal weather variations. The combination of these disparate

271   datasets, which have very different spatial and temporal resolutions and degrees of

272   uncertainty, presents some challenges, but also allows a more complete analysis of the

273   setting.

274   **3.1 Weather estimates**

275   The TRMM satellite has utilized microwave and radar instruments since late 1997

276   with a spatial coverage between latitude 50°S to 50° (Huffman, 2011). The Daily TRMM

277 Rainfall Estimate (3B42 v7) used for our analysis is a product derived from rain gauge

278 and multiple TRMM satellite measurements. First, independent precipitation estimates

279 from various microwave instruments are calibrated to TRMM Combined Instrument

280 (TCI) precipitation estimates (Huffman, 2011). The 3-hourly multi-satellite

281 measurements are combined with the accumulated monthly Global Precipitation

282 Climatology Centre (GPCC) rain gauge analysis using inverse-error-variance weighting

283 to form a monthly best-estimate precipitation rate (Huffman, 2011). Lastly, the 3-hourly

284 estimates are scaled for the month then summed to the monthly value for each individual

285 grid box (Huffman, 2011). The final data set has precipitation estimates with a 3-hourly

286 temporal resolution and a 0.25°x0.25° spatial resolution (Huffman, 2011). This temporal

287 resolution is sufficient to observe storms that can occur in the span of a few hours across

288 the surface salt structures in Kuqa fold-thrust belt.

289   Another dataset we have used includes daily humidity, temperature, and rainfall

290 measurements from a meteorological weather station in Kuqa, Xinjiang Province, China

291 (Tutiempo Network). We utilize this station, despite its location over 150 km away,

292 because it is the closest ground truth. When we compare the rainfall estimates from the

293 weather station and the TRMM dataset we look at the cumulative measurements for the

294 time periods between each Envisat image acquisition. Similarly, we compare the average

295 surface temperature and humidity during each time period between image acquisitions.

296 **3.2 Interferometry of synthetic aperture radar (InSAR)**

297   We constructed an InSAR time series to constrain the surface displacements of

298 active extruded salt structures in western Kuqa fold-thrust belt as well as several surface

299 displacements associated with hydrocarbon withdrawal and subsurface fluid injection.

300   InSAR is a remote sensing technique that uses radar imagery to provide spatially dense

301   measurements of surface displacements in the satellite line of sight (LOS) with millimeter

302   to centimeter accuracy (e.g., Zebker et al., 1994; Massonnet and Feigl, 1998; Bürgmann

303   et al., 2000). Multiple SAR images are used to generate sets of interferograms to form a

304   time series after a joint inversion (e.g., Berardino et al., 2002). InSAR time series analysis

305   helps reduce the impact of several noise sources (decorrelation, orbital and DEM errors,

306   atmospheric delays, phase unwrapping errors) on displacement rates estimates during the

307   time period spanned by the full dataset (e.g., Grandin et al., 2012) with an accuracy for

308   surface displacement velocity at the mm/yr scale. The time series analysis also allows

309   identification of time variable deformation including seasonal signals and response to

310   earthquakes or anthropogenic activity.

311   We use 40 ESA ASAR C-band radar images acquired by the Envisat satellite

312   between June 2003 and October 2010 from Track 291 (along descending orbits). A small-

313   baseline approach (e.g., Berardino et al., 2002) was used to process interferograms and

314   invert for average displacement rates and evolution through time with the New Small

315   Baseline Algorithm Subset (NSBAS) chain, as described in detail by Doin et al. (2011)

316   and Jolivet et al. (2013). 85 individual interferograms were generated using a modified

317   version of the Caltech/JPL Repeat Orbit Interferometry Package (ROI_PAC, Rosen et al,

318   2004) and the STRM 90-global DEM. Interferograms were corrected from DEM errors

319   (Ducret et al., 2013) and stratified tropospheric delays (based on the ERA-Interim global

320   atmospheric model, Doin et al., 2009; Jolivet et al., 2011), multi-looked by a factor of 4

321   in the range direction and 20 in the azimuth direction, flattened and filtered before

322   unwrapping. Individual interferogram coherence was used to determine the optimal

323   unwrapping path for each interferograms. The phase unwrapping was achieved

324   iteratively, beginning in areas of high coherence then incrementally reducing the

325   coherence threshold for each iteration (Grandin et al., 2012). The InSAR inversion

326   process does not allow for a direct measurement of the error margin of the LOS

327   displacement measurements, however we estimate the noise level is on the order of ~1

328   mm/year. Radar amplitude images were used to interpret the namakiers' boundaries,

329   outlined on the velocity maps.

330   We present average velocity (mm to cm/yr) and displacement maps with a spatial

331   resolution of 80 x 80 m. The velocity and displacement maps are displayed in line of

332   sight (LOS) with positive (red) and negative (blue) values corresponding to movement

333   toward and away from the sensor that we furthermore interpret as uplift and subsidence,

334   respectively, due to the dominant sensitivity of InSAR to vertical motion. Differential

335   incremental displacement maps and time series are used to track the temporal phase

336   evolution. To isolate relative displacements, we generate these differential maps and time

337   series computing the difference between time series from points within deforming areas

338   and times series from local reference points. This helps minimizing the effect of spatially

339   coherent noise. The remaining, relative, correlated temporal fluctuations observed and

340   comparisons to weather conditions are discussed in the following section.

341   The present study uses three datasets that were processed to obtain a time-series

342   that cover the period June 2003 to October 2010 where InSAR data provide estimates of

343   surface displacement at a pixel size of ~30 m and time resolution of 36 to 210 days, with

344   an average of 75 days. From the nearest weather station, average temperatures and

345   precipitations are obtained. Finally, the TRMM data provide the same time-lapse series as

346   the weather station, at a pixel size resolution of 4 km and for the same periods at the

347   InSAR data. These three data sets are then processed to 1) analyze the surface

348   deformation of salt bodies, 2) correlate these deformations with weather conditions.

349   **4. RESULTS**

350   **4.1 Kinematic observations**

351   The overall distribution of LOS velocity at Bozidun namakier is relatively

352   uniform. From the average velocity map, minor subsidence is observed on the western

353   margin and localized uplift near the north and east (**Figure 4A**). The velocity distribution

354   across Bozidun namakier is nearly indistinguishable from its immediate surroundings

355   supporting field observations that suggest Bozidun namakier is not actively extruding

356   material to the surface, as shown in the time series of the **Figure 4**.

357   The distribution of positive and negative LOS velocities at Daxiagu is

358   asymmetrical and ranges from -4.5 to 5 mm/yr (**Figure 4B**). An area of uplift is observed

359   on the northeastern side of the structure, oriented toward the northwest. Areas of overall

360   subsidence occur predominately on the southwestern side of the structure as well as the

361   northwestern. The incremental displacements maps highlight deformation patterns that do

362   not reflect the long-term deformation patterns measured by the average displacement

363   velocity maps (**Figure 5**). Each incremental displacement map of Daxiagu displays

364   relatively uniform deformation across the namakier with fluctuations between surface

365   uplift and subsidence at different time intervals. Time series analysis of east and west

366   Daxiagu namakier inversely mirror each other; the east is uplifting at approximately the

367   same rate (~4.5 mm/yr) as the west is subsiding. The ribbed pattern that appears in both

368   the average velocity map and the incremental displacements maps do not correlate to

369   topographical variations but instead may reflect noisiness in the data likely due to the

370   namakiers' rugged surface.

371   Displacement velocities at Awate namakier are distributed asymmetrically

372   (**Figure 4C**). Awate namakier is divided in two by a major river with stronger subsidence

373   observed on the eastern segment, slight subsidence on the west, and uplift at the river

374   channel in between. On the eastern Awate namakier the displacement velocities decrease

375   radially away from the center and the maximum rate of displacement approaches -5

376   mm/yr. Incremental displacement maps show that the east Awate namakier has

377   experienced periods of uplift despite overall subsidence suggesting it is an active

378   structure. The areas of displacement at east Awate namakier have consistent shapes in the

379   incremental displacement maps for periods of a year to three, but gradually shift from a

380   central block to a more variegated area. These areas all subside and uplift more

381   dramatically than the surroundings. Minor subsidence and unvarying incremental

382   displacements are observed at west Awate namakier. Localized uplift at the river channel

383   approaches 4 mm/yr. The zone of uplift is broader than the river channel, extending

384   farther to the west. Incremental displacement maps show uplift at the riverbed, dividing

385   Awate namakier, initiated toward the western riverbank then propagated toward the

386   center. The time series analysis at the river channel is notably less noisy and fluctuating

387   than the time series from areas across the namakier, especially for east Awate namakier

388   (**Figure 4**). This observation indicates that uplift at the river channel is relatively regular

389   and constant while displacement of the namakier is relatively irregular.

390   The distribution of average displacement velocities across Quele namakier is

391   predominately uniform (**Figure 4D**). Relative subsidence is measured along the exhumed

392   thrust sheet but strong, localized subsidence is observed at the central segment of Quele

393   namakier where the average displacement velocity approaches ~4 mm/yr. Velocities

394   measured at Chaerhan namakier and the isolated salt dome at the eastern extent of Quele

395   are within the noise level of background velocity measurements. A few periods of minor

396   uplift are observed in the incremental displacement maps at the central segment despite

397   the overall subsidence suggesting an actively extruding structure (**Figure 4**). Time series

398   analysis shows the displacement trends of two areas in the central segment partially

399   mirror each other, from 2003 to 2006. After 2006, higher rates of subsidence are

400   concentrated toward the east suggesting heterogeneities along the salt thrust.

401   **4.2 Correlation between kinematics and weather conditions**

402   To test the relationship between weather conditions and surface displacements of

403   namakiers in Kuqa fold-thrust belt we compare the incremental displacements between

404   each image acquisition to the average humidity, average temperature, and cumulative

405   rainfall during the respective time intervals (**Figure 6**). There is no clear correlation

406   between average humidity estimates and surface displacements for any of the studied

407   namakiers. Similarly, no correlation is observed between displacements and average

408   temperature for Quele namakier. Furthermore, correlation coefficients between surface

409   displacement measurements on across the 4 namakiers studied and average temperature

410   and humidity estimates yield a maximum correlation of 0.2. However, at Awate, Bozidun

411   and Daxiagu namakiers we see temperature extremes are associated with more surface

412   salt motion than intermediate temperatures. When we compare the displacements

413   observed at the namakiers to the cumulative rainfall values estimated by TRMM as well

414   as the distantly located weather station, we find a positive correlation. There is an

415   increased occurrence of surface salt displacements during time intervals that experienced

416   lower rainfall estimates suggesting that with less rainfall there is more surface motion.

417   The correlation observed is not simply an artifact of having more data during periods of

418   lower rainfall events because there are equal amounts of temporal coverage during the

419   rainy (April-October) and dry seasons (October-April).

420   Another way to test the correlation between observed surface displacements and

421   rainfall is to look at how the displacement residuals correlate to rainfall estimates. The

422   residuals of a dataset are the observed values minus the predicted (or average) values.

423   Residuals highlight the data points' deviation from the linear average, which are used to

424   test the correlation between rainfall and surface salt displacement response. When we

425   calculate the correlation coefficient between the residual time series displacements,

426   showing the deviation of each displacement data point from the average, at the namakiers

427   of interest and TRMM rainfall we find no correlation greater than 0.1. The low

428   correlation coefficient is likely due to the occurrence of both positive and negative

429   motion with hot and cold temperatures.

430   **5. DISCUSSION**

431   InSAR analysis uncovers a variety of ground motions across the subaerial salt

432   structures of the Kuqa fold-thrust belt. While the majority of the namakiers studied show

433   surface motion, InSAR estimates of surface motion at Bozidun and Chaerhan namakiers

434   are relatively indistinct from the surrounding area. The lack of observable deformation at

435   the Tuzimazha salt wall could mean that (1) the salt wall has recently become inactive,

436   (2) it is deforming at rates below our detection threshold (<1 mm/yr), or (3) the activity is

437   confined to a small area that is more challenging to resolve. We favor the third

438   interpretation because the thickness of the Tuzimazha salt wall (~50 m) cannot be

439   adequately resolved by the 80 x 80 m spatial resolution of our InSAR dataset (Figure S4).

440   The namakiers exhibit asymmetrical spatial displacement patterns with fluctuating

441   deformation rates over varying temporal scales (weeks to months). Average velocity

442   estimates in addition to the incremental displacement steps allow us to explore the

443   seasonality of subaerial salt deformation and its link to weather conditions.

444   **5.1 Daxiagu namakier**

445   The asymmetric displacement patterns observed at Daxiagu namakier (**Figure**

446   **7A**) do not conform to the expected radial flow pattern of a salt fountain. The irregular

447   shape and flow kinematics is likely controlled by the surrounding topography and sub-

448   salt morphology beyond the feeder, beneath the namakier. A river east of Daxiagu has

449   eroded steep channel walls, and likely rapidly dissolves salt that flows toward the east.

450   Because surface uplift is expected directly above the feeder (orifice) of a point-

451   source namakier, we interpret the area of overall uplift, on the eastern side of the

452   namakier, to indicate the location of the salt feeder. Long-term average uplift also

453   suggests that the rate of salt extrusion into the namakier exceeds the rate of salt

454   dissolution/erosion. The similarity in magnitude of surface displacement on the east and

455   west may indicate the two sides of the namakier are not mutually exclusive (**Figure 4**).

456   Diminutive subsidence at the northwestern margin could also indicate partial flow toward

457   the northwest from the namakiers' feeder. Eastward flow is expected, where a river

458   passes, but the material that flows toward the river is likely dissolved relatively rapidly.

459   The subsidence is interpreted to reflect an approximate volume balance as the namakier

460   spreads farther out. This interpretation suggests that the dominant direction of flow is

461   toward the west and that lateral spreading is faster than the rate of supply. The

462   southwestern lobe of Daxiagu is subsiding on average, but does not appear in the time-

463   lapse data in any one time-step. However, we find no statistical correlation to suggest

464   weather conditions control the surface motion patterns measured. Furthermore, this

465   observation is not likely to be climatically driven because we do not see it in incremental

466   displacement maps. The north-south tectonic shortening (~4-7 mm/yr) accommodated

467   across the Kuqa fold-thrust belt is likely to have a greater influence on the exhumation

468   rates and subsequent surface displacement patterns (e.g., Allen et al., 1991; Zhong and

469   Xia, 1998; Yang et al., 2010; Zubovich et al., 2010). However, to positively discriminate

470   the precise influence of regional shortening on subaerial salt motion, spatially dense GPS

471   observations are necessary across the area.

472   **5.2 Awate namakier**

473   Subsidence is concentrated at the center of the eastern Awate namakier (**Figure**

474   **7B**). The broad, long-term deformation pattern of centralized subsidence is indicative of

475   a mature namakier that is experiencing a dissolution / erosion rate which exceeds the rate

476   at which salt is fed into the structure. Distinct anthropogenic forcing may play a role: salt

477   mining operations spray water along the southwestern margin of the eastern Awate

478   namakier branch, which may influence the observed long-term subsidence by locally

479   increasing salt dissolution.

480   Incremental displacement maps do not entirely correspond with observations from

481   the average displacement velocity map, thereby revealing different deformation patterns

482   at different temporal scales. Unlike the long-term displacement pattern, four intervals of

483   incremental surface uplift at eastern Awate namakier occur between January and March

484   (colder/drier months) confirming that new material (salt) is being fed into the namakier.

485   We observe uplift when our temperature-kinematic salt models predict Awate would

486   experience overall surface subsidence during colder periods in response to thermal

487   contraction. Calculated correlation coefficients between incremental displacements and

488   temperature variations show no statistical correlation. Temperature variations do not

489   appear to control periods of wide spread uplift and subsidence. The intervals of uplift do,

490   however, support the dry-inflation model. The dry-inflation kinematic salt model predicts

491   a namakier will inflate during dry periods because the carapace inhibits lateral spreading.

492   At Awate namakier, we observe uplift above a central location (dome) during periods of

493   low rainfall implying that the carapace restricts lateral spreading and prefers dome

494   inflation during dry periods. Furthermore, periods of increased rainfall do not correspond

495   to increased surface salt uplift.

496   The average, long-term (~7.3 years) uplift signal measured at the river channel

497   between the east and west segments is not notably observed in the incremental

498   displacement maps. If river deposition were responsible for the rise of the river channel

499   surface between the Awate namakier branches, the area of uplift would not be as

500   localized as observed. Instead, the rise would continue as the river does, toward the south.

501   It is more likely that the concentrated uplift observed at the river channel is due the rise

502   of salt from the source layer through the stem of the diapir that feeds Awate namakier. If

503   the river cuts off the salt feeder that sources Awate, the observed uplift could be the result

504   of accumulating strain in the overburden of a partially buried, active salt feeder.

505   However, the estimated long-term rate of uplift here is not likely to persist for time scales

506   of >100 years because that would significantly perturb the long-term equilibrium

507   topography by developing a hill in the very place there is a river. It is possible to perturb

508   the equilibrium topography if the diapir is new or suddenly changing character, but it is

509   not new because the namakier is well established. Thus, we interpret the equilibrium to

510   be controlled by the regular frequency of large flooding events allowing this area to

511   neither rise nor fall with respect to regional baseline for longer periods than ~7 years.

512   Alternatively, the surface of the river channel in between the Awate namakier can be

513   controlled by a natural equilibrium between the diapir extrusion rate and river erosion. A

514   study of climatic conditions from 1951 to 2009 in Xinjiang, China reveals that the

515   average precipitation has increased by 15 mm since 1990 (Kong and Pang, 2012). To our

516   knowledge, a detailed study of this particular river does not exist, however, work done on

517   the proximal Tailan River, west of Awate, found that glacial melt-water accounts for 60%

518   of its $7.5 \times 10^8 \text{ m}^3$ annual river discharge (Zhao et al., 2015). The combination of

519   increased rainfall and possible glacial melt-water, due to the 1˚C raise in average annual

520   temperature, would facilitate flash-floods every 10 to 100 years that removes a lot of

521   material through erosion, maintaining a topographic equilibrium (Kong and Pang, 2012).

522   **5.3 Quele namakier**

523   Quele namakier (**Figure 7C**) is the exhumed portion of a significant salt thrust

524   and its surface kinematic patterns vary from typical salt fountains. Because it is a line-

525   source structure, we do not expect to see radial flow comparable to a point-sourced

526   structure. Unlike a salt fountain, if the exhumation rate of Quele namakier increases the

527   surface is not likely to uplift significantly because it is confined by its overburden, the

528   hanging wall of the Quele salt thrust. Instead we would see increased subsidence due to

529   amplified southward spreading. Decreased exhumation would result in stagnant to

530   minimal lateral spreading. The overall subsidence observed across Quele namakier is

531   within the range of the data resolution. However, one area of the structure has

532   experienced a higher rate of subsidence. Weather conditions are unlikely to be

533   responsible because we see no statistical relationship between surface motion and

534   weather variations (temperature and moisture). Furthermore, it is unlikely that weather

535   conditions would exclusively and consistently affect only one spot along a relatively

536   smooth hill-front. Alternatively, the isolated subsidence at Quele namakier may be

537   structurally controlled. The subsidence could be the result of a pinched salt source

538   because analog models by Cotton and Koyi (2000) show that an overriding hanging wall

539   can pinch a salt décollement during shortening. A possible indicator of a pinched salt

540   décollement includes the left-lateral tear fault that occurs in the hanging wall, coincident

541   with the area of concentrated subsidence (**Figure 7E**). The tear fault could have resulted

542   from lateral variations along the salt décollement, such as thickness, which could indicate

543   a pinched salt source for Quele namakier. Alternatively, the tear fault may be the result of

544   differential shortening of the thrust sheet. A large siliciclastic rock body, which appears

545   to be a raft, is located along Quele namakier and south of the tear fault (**Figure 7E**). If

546   this siliciclastic rock body acted as a structural barrier, limiting southward propagation of

547   the exposed Quele salt décollement (namakier), then it may have caused sufficient

548   differential shortening rates to generate a tear fault. This alternative suggests that the

549   localized, increased subsidence at Quele is the result of differential shortening across one

550   portion of the Quele thrust.

551   **5.4 Limitations**

552   Across Kuqa fold-thrust belt, we discovered that subaerial salt motion is

553 decoupled from weather conditions. The sparse temporal sampling of this Envisat dataset

554 is significantly limited when compared to the daily sampling rate of temperature and

555 rainfall from spaceborne satellites or ground-based weather stations. Additionally, the

556 restricted spatial rainfall resolution of ~4 km estimates from spaceborne satellites may

557 also preclude correlation with meter-scale InSAR sampling resolution. Looking forward,

558 the association of the European Space Agency's Sentinel 1A and 1B could provide

559 improved temporal coverage after several years of observation and better quantify the

560 temporal fluctuations that may reveal the weather dependence we expected

561 **6. CONCLUSIONS**

562   In this study we present quantitative estimates of sub-aerial salt displacement

563 rates of surface salt bodies in Kuqa fold-thrust belt of northwest China. We predicted

564 strong dependence of surface salt motion on weather conditions based on previous

565 surface salt studies but discovered weather conditions do not control surface kinematics

566 here. Although the namakiers occur in the same fold-thrust belt, none of the salt bodies

567 share the same short-term kinematic displacement pattern, which suggests contrasting

568 subsurface geometries between the salt bodies. We measure the dominant vertical

569 displacement and identify asymmetric deformation patterns of uplift and subsidence at

570 Daxiagu and Awate, likely controlled by local tectonics and topography. At Quele

571 namakier we identify an area of concentrated subsidence that is coincident with

572 surrounding structural features that may indicate a pinched salt thrust. Li et al., 2014

573 detailed the geometries of the Awate, Bozidun, Quele and Daxiagu namakiers. Our study

574   furthers our understanding of the Kuqa fold-thrust belt namakiers by providing a

575   kinematic description of the active subaerial salt motion.

576

REFERENCES

Aftabi, P., Roustaie, M., Alsop, G. I., and Talbot, C. J., 2010, InSAR mapping and modelling of an active Iranian salt extrusion: Journal of Geological Society – London, v. 167. P. 155-170.

Allen, M. B., Windley, B. F., Chi, Z., Zhong-Yan, Z., and Guang-Rei, W., 1991, Basin evolution within and adjacent to the Tien Shan Range, NW China: Journal of the Geological Society, v. 148(2), 369-378.

Baikpour, S., Zulauf, G., Dehghani, M., and Bahroudi, A., 2010, InSAR maps and time series observations of surface displacements of rock salt extruded near Garmsar, northern Iran: Journal of the Geological Society, London, v. 167, p. 171-181.

Barnhart, W.D., and Lohman, R.B., 2012, Regional trends in active diapirism revealed by mountain range-scale InSAR time series: Geophysical Research Letters, v.39, p. 1-5.

Berardino, P., Fornaro, G. and Lanari, R., 2002, A new algorithm for surface deformation monitoring based on small baseline differential SAR interferograms: IEEE Transactions on Geoscience and Remote Sensing, v. 40(11), p. 2375-2383.

Bürgmann, R., Rosen, P.A., and Fielding, E. J., 2000, Synthetic aperture radar interferometry to measure Earth's surface topography and its deformation: Annual Review of Earth and Planetary Sciences v. 28.1 p. 169-209.

Canerot, J., Hudec, M. R., and Rockenbauch, K., 2005, Mesozoic diapirism in the Pyrenean orogen: Salt tectonics on a transform plate boundary: AAPG Bulletin, v. 89(2), p. 211-229.

Chen, S., Tang, L., Jin, Z., Jia, C., and Pi, X., 2004, Thrust and fold tectonics and the role of evaporites in deformation in the Western Kuqa Foreland of Tarim Basin, Northwest China: Marine and Petroleum Geology, v. 21, p. 1027–1042.

Cotton, J.T. and Koyi, H.A., 2000, Modeling of thrust fronts above ductile and frictional detachments: Application to structures in the Salt Range and Potwar Plateau, Pakistan: Geological Society of America Bulletin, v. 112(3), p. 351-363.

Desbois, G., Závada, P., Schléder, Z., and Urai, J. L., 2010, Deformation and recrystallization mechanisms in actively extruding salt fountain: Microstructural evidence for a switch in deformation mechanisms with increased availability of meteoric water and decreased grain size (Qum Kuh, central Iran): Journal of Structural Geology, v. 32.

Doin, M. P., Lasserre, C., Peltzer, G., Cavalié, O., and Doubre, C., 2009, Corrections of stratified tropospheric delays in SAR interferometry: Validation with global atmospheric models. Journal of Applied Geophysics, 69(1), 35-50.

Doin, M-P, Lodge, F., Guillaso, S., Jolivet, R., Lasserre, C., Ducret, G., Grandin, R., Pathier, E., and Pinel, V., 2011, Presentation of the small baseline NSBAS processing chain on a case example: the Etna deformation monitoring from 2003 to 2010 using Envisat Data Proceedings from Fringe 2011 Workshop, Frascati, Italy, 19-23 September 2011(ESA SP-697, January 2012).

Ducret, G., Doin, M. P., Grandin, R., Lasserre, C., and Guillaso, S., 2014, DEM corrections before unwrapping in a small baseline strategy for InSAR time series analysis. Geoscience and Remote Sensing Letters, IEEE, 11(3), 696-700.

Grandin, R., Doin, M. P., Bollinger, L., Pinel-Puysségur, B., Ducret, G., Jolivet, R., and Sapkota, S. N., 2012, Long-term growth of the Himalaya inferred from interseismic InSAR measurement. Geology, 40(12), 1059-1062.

Hendrix M. S., Graham, S. A., Carroll A. R., Sobel, E.R., McKnight, C. L., Schulein, B. J., and Wang, Z., 1992, Sedimentary record and climatic implications of recurrent deformation in the Tian Shan: Evidence from Mesozoic strata of the north Tarim, south Junggar, and Turpan basins, northwest China: Geological Society of America Bulletin, v. 104 (1), p.

637   53-79.
638 Hudec M. R., and Jackson, M. P.A., 2007, Terra infirma: Understading salt tectonics: Earth-
639   Science Reviews, v. 82, p. 1-28.
640 Huffman, G., 2011, Global Change Master Directory - Daily TRMM and Others Rainfall
641   Estimate:http://gcmd.gsfc.nasa.gov/KeywordSearch/Metadata.do?Portal=GCMD&Metad
642   ataType=0&MetadataView=Full&KeywordPath=&EntryId=GES_DISC_TRMM_3B42_
643   daily_V7, Accessed: 07/2015.
644 Koyi, H., 1998, The shaping of salt diapirs: Journal of Structural Geology, v. 20(4), p. 321-338.
645 Jackson, M.P.A., 1985. Natural Strain in Diapiric and Glacial Rocksalt, with Emphasis
646   on Oakwood Dome, East Texas. Bureau of Economic Geology, The University of
647   Texas at Austin, Texas
648 Jackson, M. P. A., and Talbot, C. J., 1986, External shapes, strain rates, and dynamics of salt
649   structures: Geological Society of America Bulletin, v. 97, p. 305-323.
650 Jolivet, R., Grandin, R., Lasserre, C., Doin,M.-P., and Peltzer,G., 2011, Systematic InSAR
651   tropospheric phase delay corrections from global meteorological reanalysis data:
652   Geophysical Research Letters, v. 38.
653 Jolivet, R., Lasserre, C., Doin, M. P., Peltzer, G., Avouac, J. P., Sun, J., and Dailu, R., 2013,
654   Spatio-temporal evolution of aseismic slip along the Haiyuan fault, China: Implications
655   for fault frictional properties. Earth and Planetary Science Letters, 377, 23-33.
656 Kehle, R.O., 1988, The origin of salt structures. In: Schreiber, B.C. (Ed.), Evaporites and
657   Hydrocarbons. Columbia University Press, New York, pp. 345–404.
658 Kent, P. E., 1979, The emergent Hormuz salt plugs of southern Iran: Journal of Petroleum
659   Geology, v.2: p.117–144.
660 Kong, Y., and Pang, Z., 2012, Evaluating the sensitivity of glacier rivers to climate change based
661   on hydrograph separation of discharge: Journal of Hydrology, in press.
662 Li, S., Wang, X., and Suppe, J., 2012, Compressional salt tectonics and synkinematic strata of the
663   western Kuqa basin, southern Tian Shan, China: Basin Research, v. 23, p. 1-23.
664 Li, J., Webb, A. A. G., Mao, X., Eckhoff, I., Colón,C., Zhang, K., Wang, H., Li, A., He, D., 2014,
665   Active surface salt structures of the western Kuqa fold-thrust belt, Northwestern China:
666   Geosphere, v. 10 (6).
667 Massonnet, D., and Feigl, K. L., 1998 Radar interferometry and its application to changes in the
668   Earth's surface: Reviews of Geophysics, v. 36(4), p. 441-500.
669 Merriam, M. F., Smoluchowski, R., and Wiegand, D. A., 1962, High-temperature thermal
670   expansion of rocksalt: American Physical Society, v. 125
671 McGuinness, D.B. and Hossack, J.R., 1993, The development of allochthonous salt sheets as
672   controlled by the rates of extension, sedimentation, and salt supply: In Rates of
673   geological processes: 14th Annual Gulf Coast Section, SEPM Foundation Bob F. Perkins
674   Research Conference p. 127-139).
675 Talbot, C. J., and Aftabi, P., 2004, Geology and models of salt extrusion at Qum Kuh, central
676   Iran: Journal of Geological Society – London, v. 161. P. 321-334.
677 Talbot, C. J., and Jackson, M. P. A., 1987, Internal kinematics of salt diapirs: Bulletin of
678   American Association of Petroleum Geologists, v. 71(9). p. 1068-1093.
679 Talbot, C. J., and Pohjola, V., 2009, Subaerial salt extrusions in Iran as analogues of ice sheets,
680   streams and glaciers: Earth Science Reviews, v. 97(1-4), p. 155-183.
681 Talbot, C. J., and Rogers, E. A., 1980, Seasonal movements in a salt glacier in Iran. Science, v.
682   208(4442), p. 395-397.
683 Tang, L.-J., Jia, C.-Z., Jin, Z.-J., Chen, S.-P., Pi, X.-J., and Xie, H.-W., 2004, Salt tectonic
684   evolution and hydrocarbon accumulation of Kuqa fold belt, Tarim Basin, NW China:
685   Journal of Petroleum Science and Engineering, v. 41, p. 97-108.
686 Trusheim, F., 1960, Mechanism of salt migration in northern Germany: Bulletin of the American
687   Association of Petroleum Geologists, v.A(9) p. 1519-1540.

688 Tutiempo Network, S.L., "Climate KUQA - Climate Data 1956 – 2015." *TuTiempo.net.*
689   November 2015 (updated). Accessed: December 2014. URL: en.tutiempo.net/climate/ws-
690   516440.html.
691 Urai, J. L., C. J. Spiers, H. J. Zwart, and G. S. Lister, 1986, Weakening of rock salt by water
692   during long-term creep: Nature, v. 324, p. 554-557.
693 Walker, C. W., 1973, Nature and Origin of Caprock Overlying Gulf Coast Salt Domes: Fourth
694   International Symposium on Salt–Northern Ohio Geological Society. p. 169-195.
695 Wang, X., Suppe, J., Guan, S., Hubert-Ferrari, A., Gonzalez-Mieres, R., and Jia, C., 2011,
696   Cenozoic structure and tectonic evolution of the Kuqa fold belt, southern Tianshan,
697   China, in K. McClay, J. H. Shaw, and J. Suppe, eds., Thrust fault-related folding: AAPG
698   Memoir 94, p. 215-243.
699 Weijermars, R., Jackson, M.P.A., and Vendeville, B., 1993, Rheological and tectonic modeling
700   of salt provinces: Tectonophysics, p. 143–174.
701 Weinberg, R. F., 1993, The upward transport of inclusions in Newtonian and power-law salt
702   diapirs: Tectonophysics, v. 228. p. 141-150.
703 Weinberger, R., Lyakhovsky, V., Baer, G., and Begin, Z. B., 2006, Mechanical modeling and
704   InSAR measurements of Mount Sedom uplift, Dead Sea basin: Implications for effective
705   viscosity of rock salt: Geochemistry, Geophysics, Geosystems, v. 7(5).
706 Wenkert, D., 1979, The flow of salt glaciers: Geophysical Research Letters, v. 6(6).
707 Wu, Z., Yin, H., Wang, X., Zhao, B., and Jia, D., 2013, Characteristics and deformation
708   mechanism of salt-related structures in the western Kuqa depression, Tarim basin:
709   Insights from scaled sandbox modeling: Tectonophysics, v. 613-614, p. 81-96.
710 Yang, S., Li, J., and Wang, Q., 2010, The deformation pattern and fault rate in the Tianshan
711   Mountains inferred from GPS observations: Science in China Series D: Earth Sciences, v.
712   51(8), p. 1064-1080.
713 Yixin, Y. and Pengwan, W., 2009, Balanced Cross-sections of Salt Structures in Kuqa Foreland
714   Thrust Belt in Northern Part of Tarim Basin: Journal of Marine Origin Petroleum
715   Geology, p.012.
716 Zebker, H. A., Rosen, P. A., Goldstein, R. M., Gabriel, A., and Werner, C., 1994, On the
717   derivation of coseismic displacement fields using differential radar interferometry: the
718   Landers earthquake: Journal of Geophysical Research, v. 99(B10), p. 19,617-19,634.
719 Zhong, D., and Xia, W. S., 1998a, The investigation report of Mesozoic–Cenozoic strata,
720   structure, sedimentary faces, and petroleum potential of Kuche foreland basin outcrop
721   area (with 1:100,000 Kuche foreland basin geologic map): Research report of Tarim
722   Oilfield Company, Xinjiang, p. 462.
723 Zubovich, A. V., Wang, X. Q., Scherba, Y. G., Schelochkov, G. G., Reilinger, R., Reigber, C.,
724   and Beisenbaev, R. T., 2010, GPS velocity field for the Tien Shan and surrounding
725   regions: Tectonics, v. 29(6).

726 **FIGURE CAPTIONS**

727 **Colón et al., Figure 1** (Top) Geologic map of the western Kuqa fold-thrust belt, adapted

728 from Li et al., 2014, located south of Tian Shan Mountain Range and northern Tarim

729 Basin. Blue and green units toward the north represent Tian Shan bedrock. Yellow and

730 orange units represent Cenozoic basin deposits. (Bottom) Cross section (adapted from Li

731 et al., 2012) from the southern Tian Shan through the Kuqa fold-thrust belt, toward the

732 Tarim basin and dissects the Quele salt nappe and the Misikantage anticline. The

733 schematic cross section of Quele namakier is more representative of the central portion of

734 Quele namakier.

735

736 **Colón et al., Figure 2** Chart highlights variables that may control subaerial salt motion,

737 their temporal and spatial ranges, and an illustration and description of the predicted

738 kinematic impact. White arrows represent dominant salt flow direction. Black arrows

739 represent surface displacement direction. Swelling of the salt in hot weather due to

740 thermal expansion and deflation during cold weather because of thermal contraction may

741 occur however the range of motion may be very small. During and shortly after rainfall

742 events surface salt flow is predicted to accelerate significantly albeit short lived. During

743 dry periods, 2 opposing models explain surface salt behavior: Dryness (a) predicts the

744 strong carapace that develops during dry periods inhibits lateral spreading and facilitates

745 swelling at the dome (above the orifice) as the salt extrudes from the feeder. Dryness (b)

746 predicts that the thick carapace hinders uplift of the central dome and instead promotes

747 lateral spreading. The presence of a thin weak overburden/carapace can potentially

748   reduce overburden stress and accelerate salt extrusion. A thick, strong

749   overburden/carapace may apply enough overburden stress to reduce salt extrusion rates.

750

751   **Colón et al., Figure 3** Logarithmic plot with spatial range in meters over temporal range

752   in days. The yellow, green and blue regions represent the range of temporal and spatial

753   scales that deformation in response to respective variables could be observed. The purple

754   highlights possible GPS sampling resolution. The dashed black rectangle represents the

755   range of spatial and temporal sample of our Envisat dataset. Satellites like the Sentinel

756   1A and 1B have potential to reach temporal resolution of up to 5 days. The dashed gray

757   rectangle represents the maximum Tropical Rainfall Measuring Mission (TRMM)

758   resolution used in this study.

759

760   **Colón et al., Figure 4** (Top) Average surface velocity maps for Bozidun namakier (A),

761   Daxiagu namakier (B), Awate namakier (C), and Quele namakier (D) displayed in

762   satellite line of sight (LOS) and saturated to the color scale 0.5 to -0.5 cm/yr. Surface

763   movement toward (uplift) and away (subsidence) from the satellite is represented by

764   warm and cool colors, respectively. (Bottom) Differential time series analysis of select

765   points on Bozidun, Daxiagu, Awate, and Quele namakiers (locations are highlighted by

766   black circles on the velocity maps above) is displayed in LOS displacement (cm) across

767   time (from June 2003 to October 2010). The displacement measurements are relative to

768   local references represented by the label "Ref".

769

770 **Colón et al., Figure 5** Line-of-sight (LOS) differential incremental displacement maps of

771 Daxiagu (1A-33A), Awate (1B-33B), and Quele namakiers (1C-33C), saturated to the

772 color scale 5 to -5 cm. Displacement values of the local reference points (labeled in

773 Figure 4) were removed from each incremental displacement map (*Ref1* was used for

774 Quele namakier) to reduce spatially coherent noise and highlight relative motion. Each

775 incremental map spans the time between 2 successive acquisitions, the temporal coverage

776 is represented by the shaded red area on each timeline.

777

778 **Colón et al., Figure 6** Comparison between surface displacements at Kuqa fold-thrust

779 belt and weather conditions. We evaluate the dependence of incremental LOS

780 displacement rates (cm) from each structure (Bozidun, Daxiagu, Awate, and Quele

781 namakiers) to daily humidity (left), temperature (center left), and rainfall/snowmelt

782 measurements (center right) at a meteorological weather station in Kuqa (Xinjiang

783 Province, China) from Tutiempo Network and daily cumulative rainfall estimates from

784 the Tropical Rainfall Measuring Mission (right).

785

786 **Colón et al., Figure 7** (Top) Schematic cross-section and overview of displacement

787 patterns across Daxiagu, Awate and Quele namakiers and kinematic interpretations.

788 Daxiagu is interpreted to have an inflating dome that actively extrudes from salt feeder on

789 the eastern side. Similarly, Awate is interpreted to flow predominantly toward the east to

790 southeast. Awate is interpreted to have a salt feeder on the eastern segment that may be

791 partially buried by the adjacent river channel causing the localized uplift. Unlike Awate

792 and Bozidun namakiers, Quele namakier does not have a central dome because it is an

793   exhumed salt thrust décollement. We interpret the dominant flow direction of Quele

794   namakier to be toward the south. (Bottom) The average displacement map (displayed in

795   radians) overlaid on top of Google Earth. The concentrated area subsidence at Quele

796   corresponds precisely to a large raft immediately to the east of the area of deformation.

797   The local left-lateral tear fault may also have created a structure barrier between this part

798   and the rest of the namakier.

FIGURES
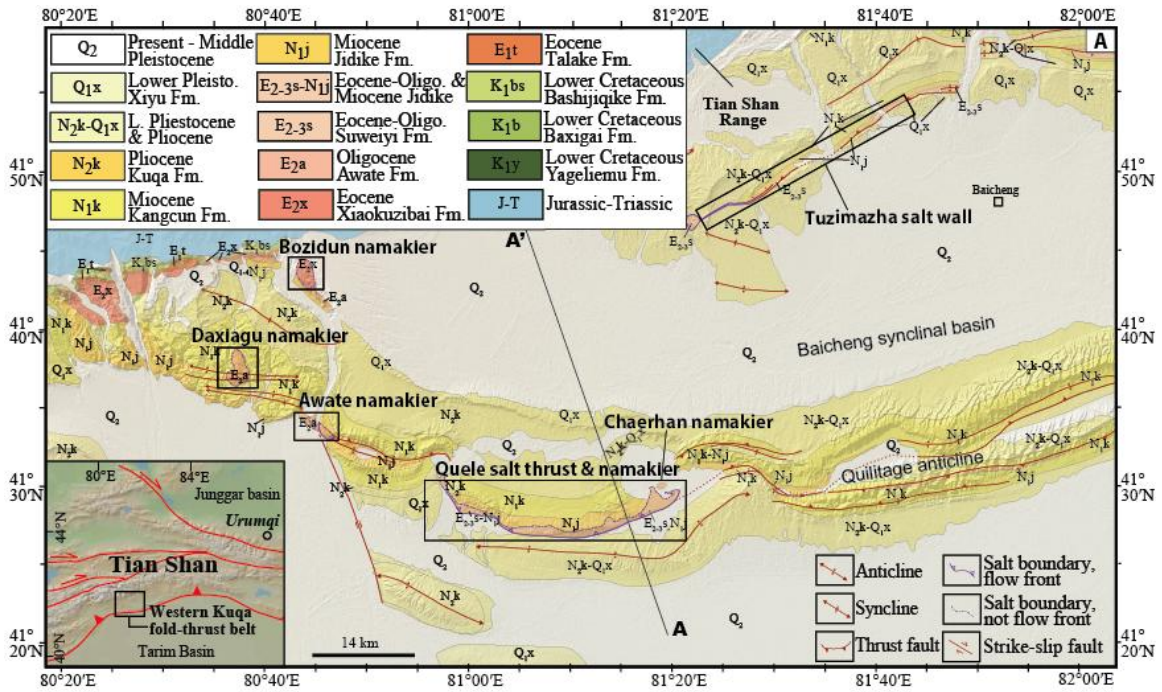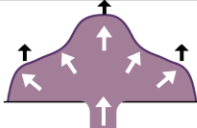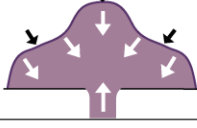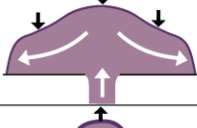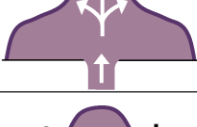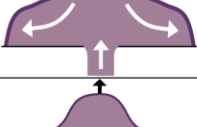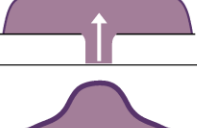
(B) Kuqa fold-thrust cross-section
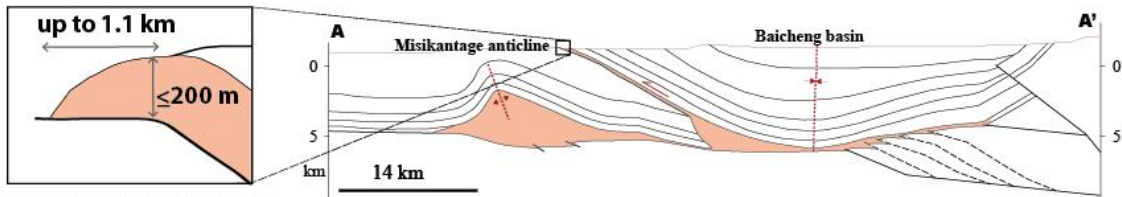
Schematic cross-section of Quele
namakier (central segment)

Colón et al., Figure 1

Factors impacting subaerial salt structure motion

| Variable	Temporal range	Spatial flow range	Kinematic response to external condition
Hot (surface temp.)	hourly, daily, seasonal	<mm to cm	Thermal expansion may cause inflation and overall relative surface uplift of the namakiers when surface temperatures are high
Cold (surface temp.)	hourly, daily, seasonal	<mm to cm	Thermal contraction may cause deflation and overall relative surface subsidence of the namakier when temperatures are low
Wetness	daily, seasonal	<mm to meters	Meteoric waters facilitates pressure-solution GBS which accelerates salt flow. As salt spreads faster and further laterally, the namakiers' surface appears to subside
Dryness (*a*)	seasonal	<mm to cm	Dry-inflation scenario suggests the carapace, developed during dry periods, inhibits lateral spreading and facilitates swelling above the orifice resulting in relative surfac uplift above the orifice
Dryness (*b*)	seasonal	<mm to cm	Dry-deflation scenario suggests the carapace, developed during dry periods, hinders uplift of the central dome and promotes lateral spreading resulting in surface subsidence of the namakier as it spreads laterally
Thin Overburden	seasonal, annually	<mm to cm	If enough material is removed from the top of a namakier, thereby reducing the overburden above the orifice, and causing an increase salt extrusion rate which results in surface uplift above the orifice
Thick Overburden	>annually	<mm to cm	If a namakier carapace thickens significantly then the additional load from may cause enough resistance to decrease the salt extrusion rate resulting in reduced namakier growth

= vertical surface motion   = dominant salt flow direction
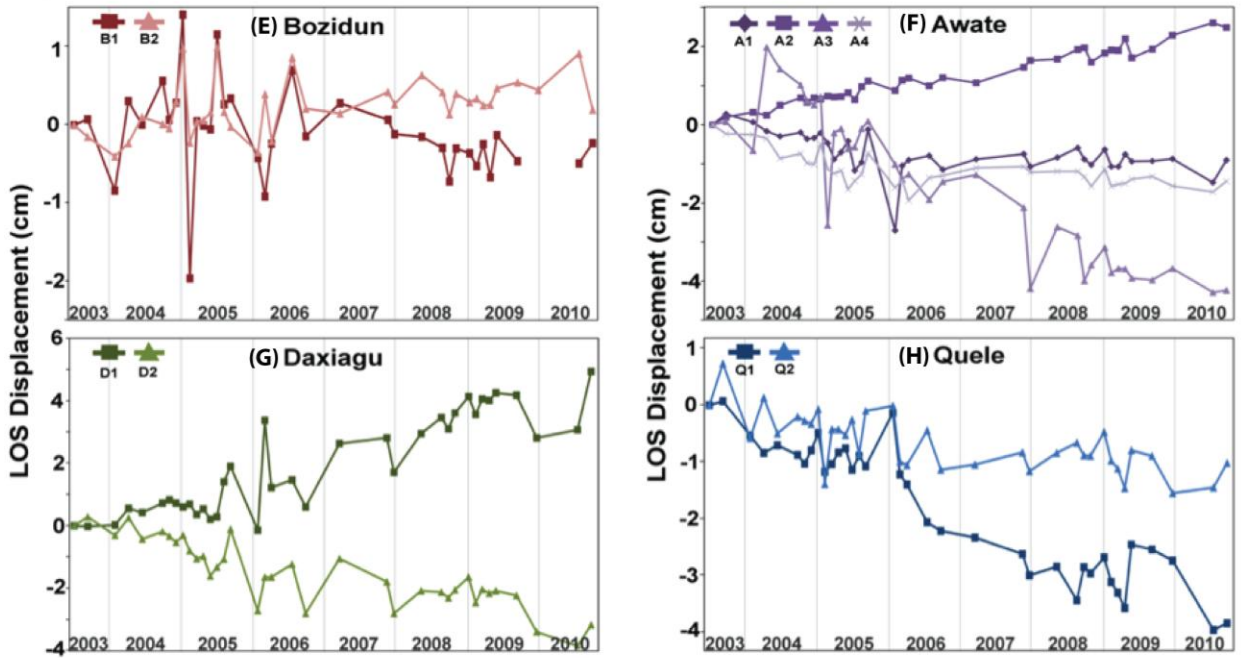
Colón et al., Figure 2
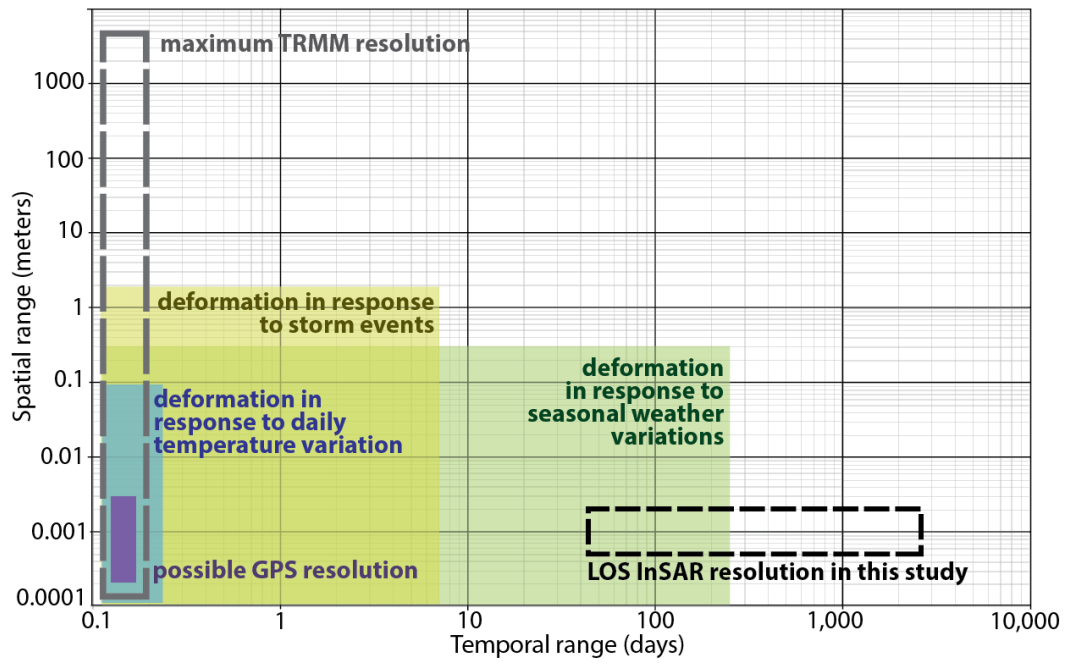
Colón et al., Figure 3
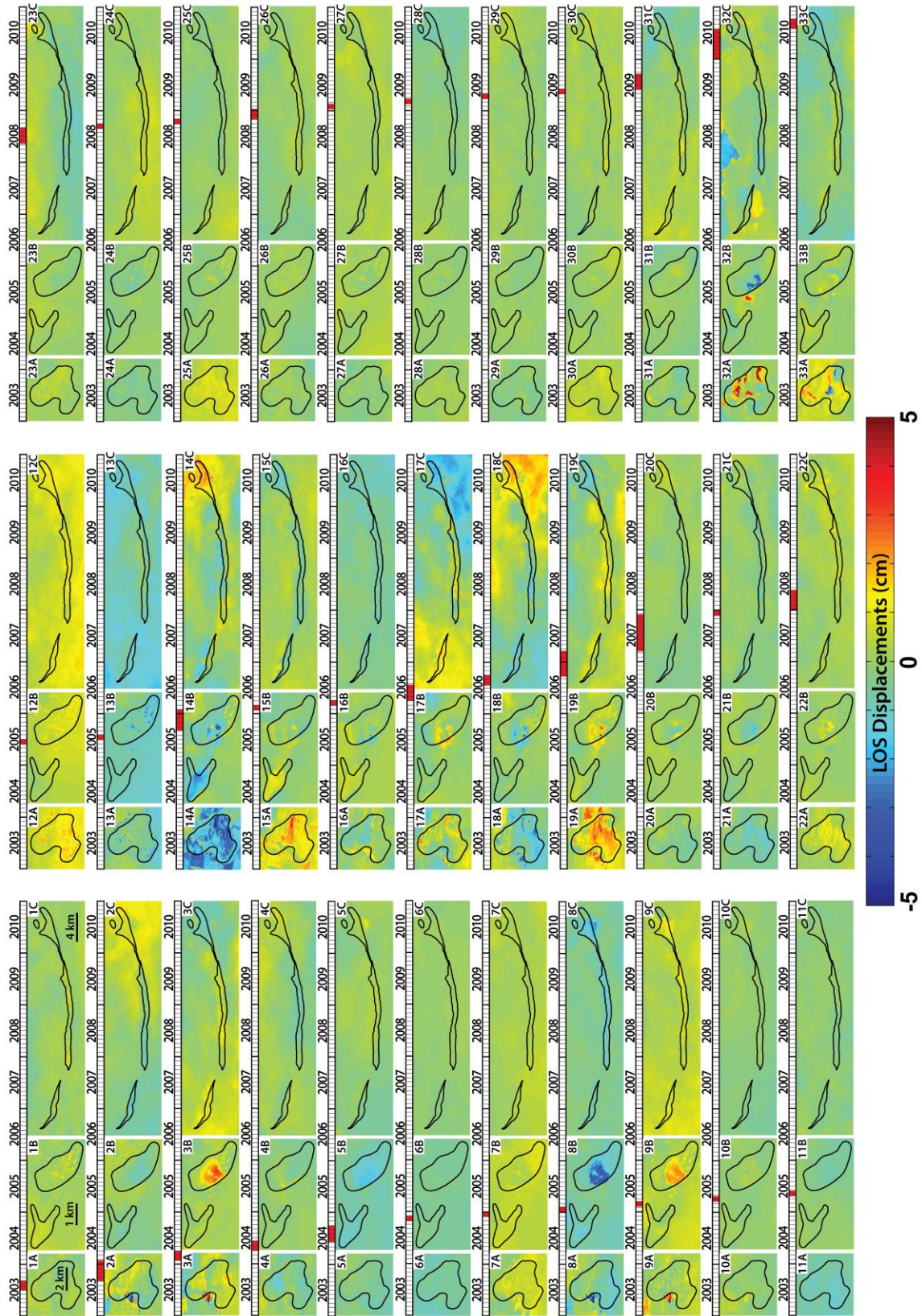
Average surface displacement rate maps

(A) Bozidun namakier

(B) Daxiagu namakier

(C) Awate namakier

(D) Quele namakier
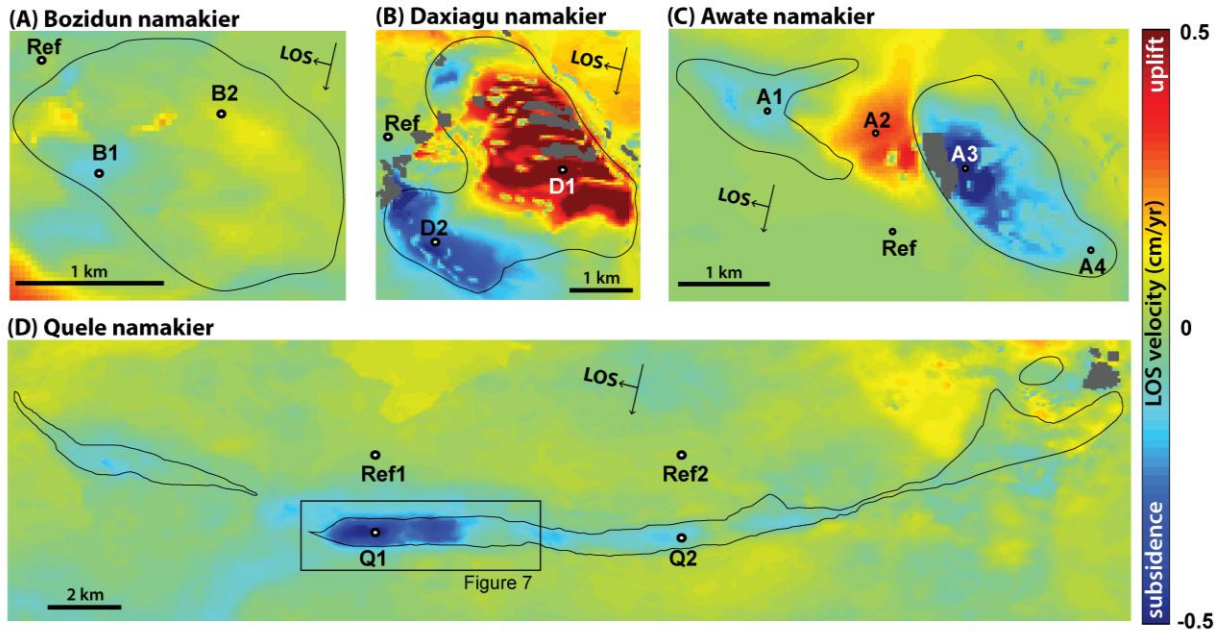
Time series analysis of surface salt structures
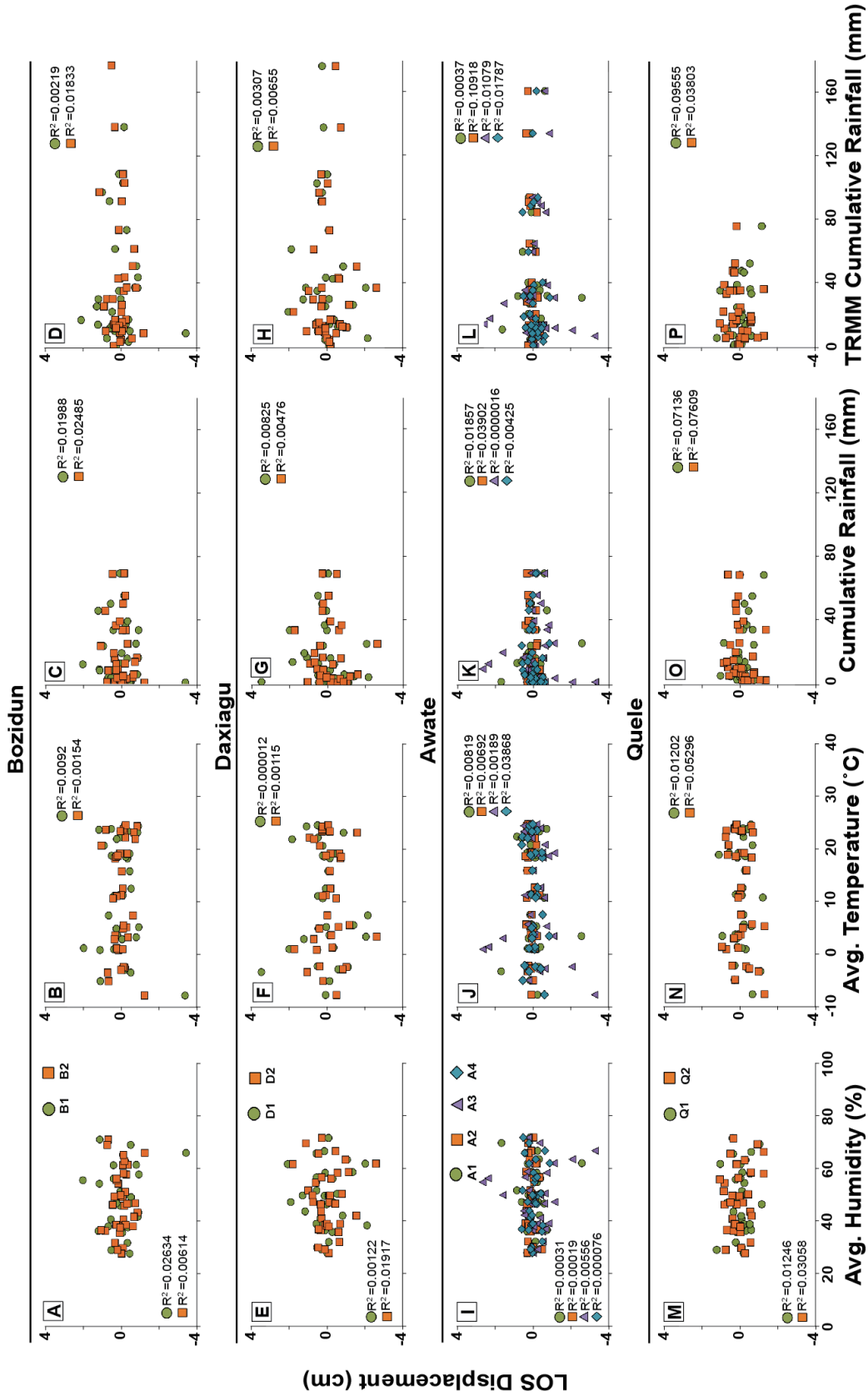

(E) Bozidun

(F) Awate

(G) Daxiagu
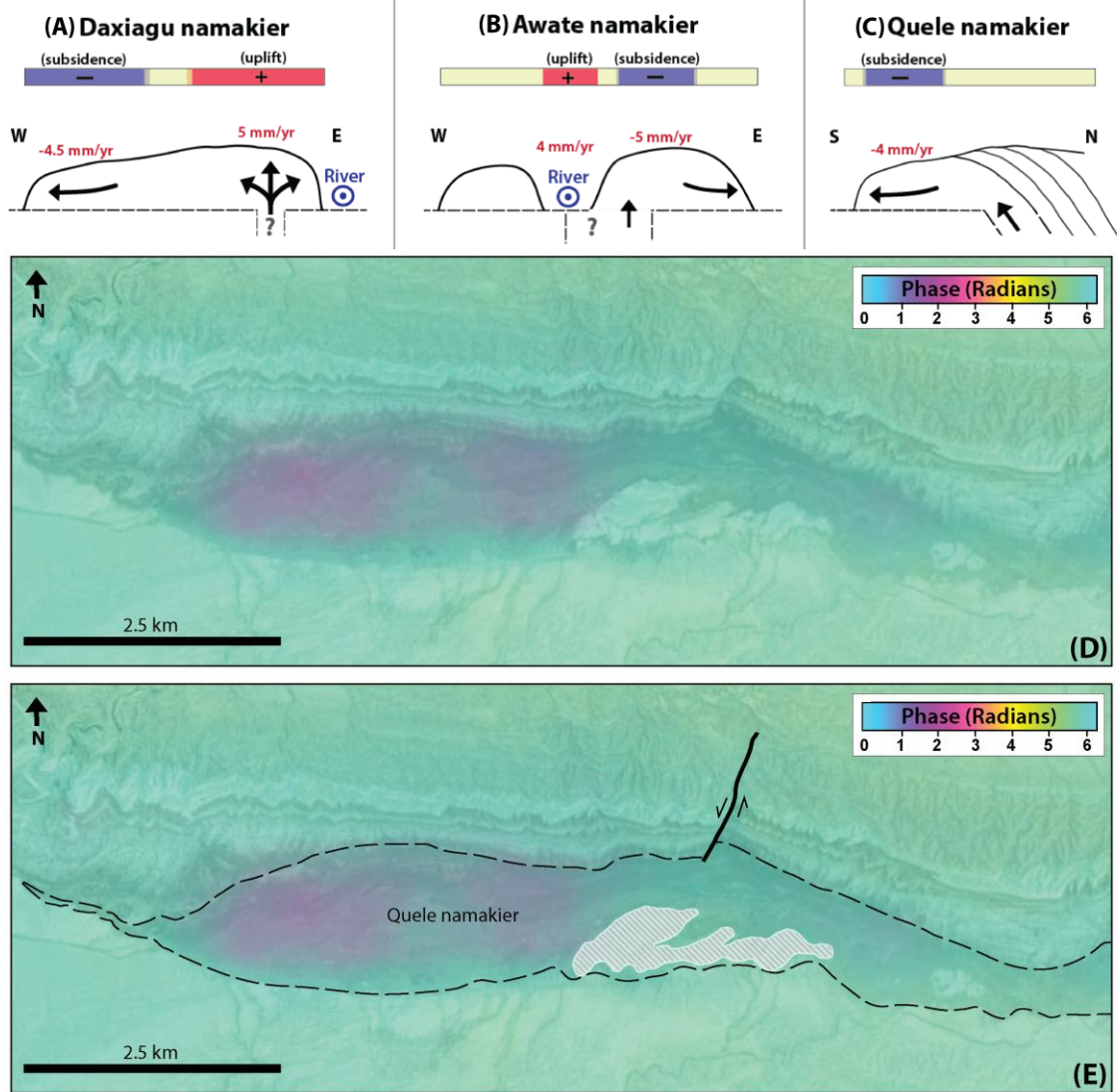
(H) Quele

Colón et al., Figure 4

Colón et al., Figure 5

Colón et al., Figure 6

InSAR surface displacement rates and kinematic interpretations

(A) Daxiagu namakier

(subsidence) — (uplift) +

W -4.5 mm/yr 5 mm/yr E River

?

(B) Awate namakier

(uplift) + (subsidence) —

W 4 mm/yr -5 mm/yr E River

?

(C) Quele namakier

(subsidence) —

S -4 mm/yr N

Phase (Radians)
0 1 2 3 4 5 6

N

2.5 km

(D)

Phase (Radians)
0 1 2 3 4 5 6

N

Quele namakier

2.5 km

(E)

Colón et al., Figure 7